DOI: 10.1002/ejic.200900255

A Structural and Magnetic Study of the Series of Double Perovskites $Ca_2Fe_{1+x}W_{1-x}O_6$

María Retuerto,*[a] José Antonio Alonso,[a] María Jesús Martínez-Lope,[a] Mar García-Hernández,[a] Carlos A. López,[b] María del Carmen Viola,[b] José C. Pedregosa,[b] and María Teresa Fernández-Díaz[c]

Keywords: Perovskite phases / Neutron diffraction / Structure elucidation / Magnetic properties

The synthesis of the $Ca_2Fe_{1+x}W_{1-x}O_6$ perovskite solid solution in the range $x = 0.13$–0.33 by a soft-chemistry procedure followed by annealing at different temperatures under different reducing atmospheres, and its characterization by X-ray and neutron diffraction together with magnetic measurements, is reported. The average Fe oxidation state in this series varies smoothly from $Fe^{2.46+}$ in $Ca_2Fe_{1.13}W_{0.87}O_6$ to Fe^{3+} in $Ca_2Fe_{1.33}W_{0.67}O_6$. A detailed description of the crystal structure of four selected members of this series ($x = 0.2$, 0.23, 0.30, 0.33) is provided. All these compounds crystallize in the space group $P2_1/n$, with $\mathbf{a} \approx \mathbf{b} \approx \sqrt{2}\mathbf{a_0}$ and $\mathbf{c} \approx 2\mathbf{a_0}$, although they show different levels of long-range ordering between the two different cations placed at the B positions of the $A_2B'B''O_6$ perovskite structure. The driving force for this B′/B″ ordering is the charge difference between both kinds of cations, whereby the earlier members of the series, which contain a large proportion of Fe^{2+}, are fully ordered whereas a strong antisite disorder effect is observed for the later members. The evolution of this antisite disordering has a dramatic influence on the magnetic properties across the series. Thus, for $x = 0.20$, the ferrimagnetic Curie temperature is above 400 K, although the saturation magnetization is very low, since there is a poor coherence between the antiferromagnetic patches formed by Fe–O–Fe interactions between the B′ and B″ positions of the perovskite, whereas the $x = 0.33$ compound, which has a lower T_C of 310 K, shows a considerable saturation magnetization and a surprisingly strong magnetic neutron scattering for such a structurally disordered sample. The observed scattering can be ascribed to the good coherence obtained via Fe–O–Fe superexchange interactions among the Fe-rich, antiferromagnetically ordered patches that occur naturally thorughout the crystal.

Introduction

Interest in double perovskites ($A_2B'B''O_6$) has been renewed since the report of room-temperature magnetoresistance and half-metallic conduction properties in Sr_2FeMoO_6. This perovskite is a ferrimagnet with a Curie temperature (T_C) of 415 K.[1] Modification of the structural and magnetic properties of this kind of double perovskite by substitution at the A, B′ or B″ cation sites has been widely studied over the last few years in order to better understand the mechanisms of the magnetoresistance and to optimize their properties of interest.[2–6] Thus, closely related perovskites of composition Ba_2FeMoO_6 and Ca_2FeMoO_6 have been described, as has Sr_2FeWO_6 and the solid solution $Sr_2FeMo_{1-x}W_xO_6$,[7] where a transition from a half-metallic ferromagnet ($x = 0$) to an antiferromagnetic insulator is observed as the W content increases.[8,9] However, the Ca_2FeWO_6 perovskite is difficult to stabilize and it has rarely been studied.[10] When Ca^{2+} cations occupy the A position of the perovskite, the structural symmetry lowers considerably compared with Sr-based double perovskites and the magnetic properties are altered. For instance, Ca_2FeMoO_6 and Ca_2FeReO_6 have been reported to be monoclinic, whereas their Sr analogues are tetragonal, and the ferrimagnetic transition temperatures are also considerably modified.[11,12]

During our attempts to isolate the material Ca_2FeWO_6, we found a solid solution of stoichiometry $Ca_2Fe_{1+x}W_{1-x}O_6$, where the average oxidation state of Fe could nominally be varied from Fe^{2+} in Ca_2FeWO_6 to Fe^{3+} in $Ca_3Fe_2WO_9$. Materials of stoichiometry $A_3B_2B''O_9$ are also double perovskites [rewritten as $A_2(Fe)_{B'}(Fe_{0.33}B''_{0.66})_{B''}O_6$] with intrinsic partial disorder over half of the perovskite B positions (B″). In fact, one way to enhance T_C in double perovskites is to increase the amount of Fe at the B positions in this family of materials of the type $A_3Fe_2B''O_9$ (A = Ca, Sr, Ba; B″ = transition metal).[13–15] Ivanov et al.[16] have described the structure and magnetic properties of the end member $Ca_3Fe_2WO_9$. In order to extend this study to the members of the $Ca_2Fe_{1+x}W_{1-x}O_6$ solid solution system in the range $x = 0.13$–0.33, herein we report their synthesis

[a] Instituto de Ciencia de Materiales de Madrid, C.S.I.C., Cantoblanco, 28049 Madrid, Spain
[b] Departamento de Química, Universidad Nacional de San Luis, Chacabuco y Pedernera, 5700 San Luis, Argentina
[c] Institut Max Von Laue Paul Langevin, 38042 Grenoble, France

by a soft-chemistry procedure under different reducing atmospheres, and their characterization by X-ray and neutron diffraction together with magnetic measurements.

Results

Attempts to obtain the end term of the series (Ca_2FeWO_6) by annealing the precursors under suitable reducing conditions for the stabilization of Fe^{2+} were always unsuccessful. However, we always observed the formation of $CaWO_4$ as an impurity so we assumed that the material was deficient in Ca and W (i.e. rich in Fe) and contained different materials of the $Ca_2Fe_{1+x}W_{1-x}O_6$ series. The preparation of different compositions of this series starting with the appropriate stoichiometric amounts led to pure and well-defined oxides. We observed that the stabilization of different values of x using the same reducing flow (5% or 1% H_2) requires an increase of the synthesis temperature for decreasing x values. We prepared the series with x spanning from 0.13 to 0.33 starting with the appropriate cationic stoichiometries. As described in the Experimental Section, for x = 0.33 the sample $Ca_3Fe_2WO_9$ [rewritten as $Ca_2Fe(Fe_{0.33}W_{0.66})O_6$] contains 100% Fe^{3+} and can be stabilized in air. Table 1 lists the different compounds synthesized along with the corresponding average Fe oxidation state and unit-cell parameters for each x value.

Crystal Structure

The samples were initially characterized by X-ray diffraction and the crystal structures refined by the Rietveld method. All the diffraction patterns can be fitted in the $P2_1/n$ space group, in contrast to the previously reported $Pmm2$ orthorhombic space group described for Ca_2FeWO_6.[10] Figure 1 illustrates the XRPD patterns for x = 0.2, 0.23, 0.3 and 0.33; the three former patterns show well-defined superstructure reflections (011) and (013) arising from the Fe/W ordering over both B positions due to the charge difference between Fe^{2+}–Fe^{3+} and W cations, whereas the sample with x = 0.33 shows much weaker superstructure reflections. Disorder over the two sites, due to the smaller charge difference between Fe^{3+} and W^{6+}, reduces the difference in scattering power and hence the intensity of the reflections. Figure 2 shows the variation of the unit-cell parameters and the unit-cell volume vs. the evolution of the Fe average oxidation state along the series. The volume and the cell parameters decrease as the average oxidation state of Fe increases (as x increases) due to the smaller radius of Fe^{3+} (0.645 Å) compared to Fe^{2+} (0.78 Å), which compensates the increment of the Fe content with respect to W^{6+} (0.60 Å).[17]

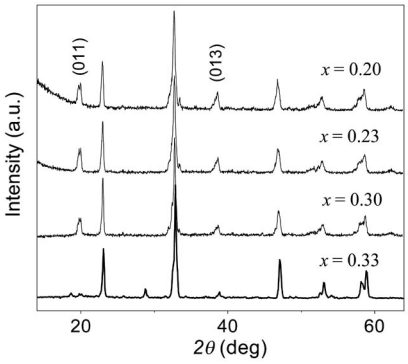

Figure 1. XRPD patterns of the members of the series $Ca_2Fe_{1+x}W_{1-x}O_6$ (x = 0.2, 0.23, 0.3 and 0.33).

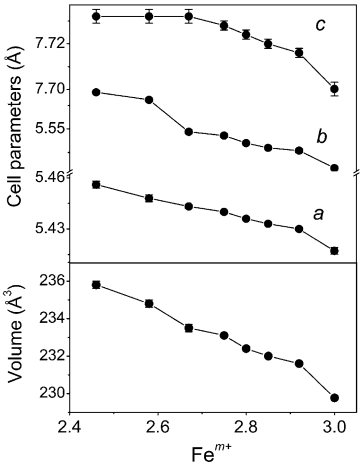

Figure 2. Variation of the unit-cell parameters and unit-cell volume vs. the nominal oxidation state of Fe cations.

An NPD study proved useful for investigating the crystalline and magnetic structures of four selected members of the series $Ca_2Fe_{1+x}W_{1-x}O_6$ with x = 0.2, 0.23, 0.3 and 0.33 at room temperature. The crystal structure of the samples was successfully refined in the monoclinic $P2_1/n$ space group (tilting system $a^-a^-c^+$, with $\mathbf{a} \approx \mathbf{b} \approx \sqrt{2}\mathbf{a_0}$ and $\mathbf{c} \approx 2\mathbf{a_0}$),

Table 1. Members of the $Ca_2Fe_{1+x}W_{1-x}O_6$ series, values of x, nominal average iron oxidation state (m+), cell parameters and volume of each sample after the Rietveld refinement of the crystal structures from XRPD data collected at room temp. (space group $P2_1/n$).

Formula	x	Fe^{m+}	a [Å]	b [Å]	c [Å]	V [Å^3]
$Ca_2Fe_{1.13}W_{0.87}O_6$	0.13	2.46	5.456(2)	5.589(2)	7.732(3)	235.8(2)
$Ca_2Fe_{1.17}W_{0.83}O_6$	0.17	2.58	5.448(2)	5.581(2)	7.732(3)	234.8(2)
$Ca_2Fe_{1.2}W_{0.8}O_6$	0.2	2.67	5.443(2)	5.547(2)	7.732(3)	233.5(2)
$Ca_2Fe_{1.23}W_{0.77}O_6$	0.23	2.75	5.440(1)	5.543(2)	7.728(2)	233.1(1)
$Ca_2Fe_{1.25}W_{0.75}O_6$	0.25	2.8	5.436(1)	5.535(2)	7.724(2)	232.4(1)
$Ca_2Fe_{1.27}W_{0.73}O_6$	0.27	2.85	5.433(1)	5.530(2)	7.720(2)	232.0(1)
$Ca_2Fe_{1.3}W_{0.7}O_6$	0.3	2.92	5.430(1)	5.527(2)	7.716(2)	231.6(1)
$Ca_2Fe_{1.33}W_{0.67}O_6$	0.33	3.00	5.417(1)	5.508(2)	7.700(3)	229.8(1)

based upon the structural model of Ca_2FeMoO_6.[11] As $P2_1/n$ is not the only monoclinic possibility in double perovskites,[18] we also checked $I2/m$ (tilting system $a^0b^-b^-$, $\mathbf{a} \approx \mathbf{b} \approx \sqrt{2}\mathbf{a_0}$ and $\mathbf{c} \approx 2\mathbf{a_0}$) and $C2/c$ (tilting system $a^0b^+c^-$, with $\mathbf{a} \approx \mathbf{b} \approx \mathbf{c} \approx 2\mathbf{a_0}$). A pattern matching in these space groups readily showed that some reflections were not indexed, therefore they were both discarded to describe the crystal structure. The $P2_1/n$ model contains two positions for Fe and W and three kinds of nonequivalent oxygen atoms (O1, O2 and O3). The observed symmetry reduction of the adopted space group is mainly due to significant tilts of the BO_6 octahedra, involving shifts of the oxygen positions, which can be suitably detected by neutron diffraction. Figure 3 shows a plot of the crystal structure, highlighting the tilting of the (Fe, W)O_6 octahedra. Refinement in the monoclinic model gave acceptable reliability factors (Table 2). Figure 4 illustrates the quality of the agreement between observed and calculated NPD profiles for the materials at room temperature. The second line of Bragg reflections corresponds to a minor impurity of $Ca_2Fe_2O_5$ for the samples with x = 0.2, 0.23 and 0.3 and $CaWO_4$ for x = 0.33.The third line of Bragg reflections corresponds to the magnetic structure, since these samples are magnetically ordered above room temperature, as discussed below.

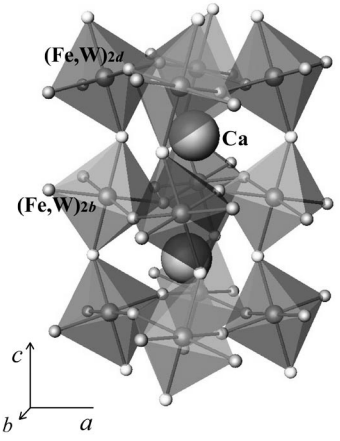

Figure 3. View of the structure of the monoclinic $Ca_2Fe_{1+x}W_{1-x}O_6$ perovskites approximately along the b axis. Large spheres represent Ca; corner-sharing (Fe, W)O_6 octahedra at the 2d and 2b sites are tilted in order to optimize the Ca–O bond lengths.

The structural parameters at room temperature are listed in Table 2. The variation of the unit-cell parameters and volume is in good agreement with the values obtained by XRPD: as the average oxidation state of Fe increases, the unit-cell parameters decrease due to the smaller radius of Fe^{3+} compared to Fe^{2+}. Table 2 also lists the atomic positions, the atomic displacement parameters, the ordered magnetic moments of Fe and the agreement factors. The degree of Fe/W ordering is defined as d.o. = (1-*asd*) × 100, where the parameter *asd* (antisite disordering) is the fraction of W atoms at Fe positions. Note that *asd* would have a value of 0.5 for a completely disordered sample. The samples with x = 0.2 and 0.23 are therefore completely ordered (100%), the sample with x = 0.3 has 93% order and the sample with x = 0.33 has 78% order.

Table 2. Positional and atomic displacement parameters and agreement factors for $Ca_2Fe_{1+x}W_{1-x}O_6$ (x = 0.2, 0.23, 0.3 and 0.33) after the Rietveld refinement of NPD data collected at room temp. (space group $P2_1/n$).

	x = 0.2	x = 0.23	x = 0.3	x = 0.33
Fe^{m+}	2.67	2.75	2.92	3.00
a [Å]	5.4439(5)	5.4418(5)	5.4323(4)	5.4171(1)
b [Å]	5.5469(5)	5.5432(5)	5.5288(5)	5.5084(2)
c [Å]	7.7363(7)	7.7314(7)	7.7178(7)	7.7002(2)
V [Å^3]	233.49(5)	233.01(4)	231.60(5)	229.77(1)
β [°]	90.027(3)	90.049(3)	90.032(2)	90.009(3)
Ca 4e(x y z)				
x	0.9814(18)	0.9936(17)	0.9900(14)	0.9928(7)
y	0.0413(8)	0.0410(8)	0.0386(7)	0.0442(3)
z	0.2390(17)	0.2350(15)	0.2362(11)	0.254(2)
B [Å^2]	0.9(1)	1.2(1)	0.51(9)	1.52(5)
Fe/W 2d (1/2 0 1/2)				
B [Å^2]	0.21(7)	0.40(6)	0.96(6)	0.9(1)
Mag. mom. [μ_B/atom]	2.1(2)	1.7(3)	1.9(3)	1.3(2)
Occupancy[a]				
Fe 2d	1.0	1.0	0.93(1)	0.78(2)
W 2d	0	0	0.07(1)	0.22(2)
Fe/W 2b (1/2 0 0)				
B [Å^2]	0.21(7)	0.40(6)	0.96(6)	0.9(1)
Mag. mom. [μ_B/atom]	0.0(2)	–0.2(3)	–0.3(3)	–0.4(2)
Occupancy[a]				
Fe 2b	0.20(2)	0.23(2)	0.37(3)	0.55(3)
W 2b	0.80(2)	0.77(2)	0.63(3)	0.45(2)
O1 4e(x y z)				
x	0.0873(11)	0.0879(1)	0.08620(8)	0.0801(4)
y	0.4734(9)	0.4756(9)	0.48151(8)	0.479(4)
z	0.2568(17)	0.2526(16)	0.25119(13)	0.251(2)
B [Å^2]	1.4(1)	1.7(1)	0.76(8)	1.17(4)
O2 4e(x y z)				
x	0.704(2)	0.7051(17)	0.7040(2)	0.7091(3)
y	0.2856(16)	0.2872(16)	0.2897(2)	0.2914(2)
z	0.0505(14)	0.0535(11)	0.0556(1)	0.0444(1)
B [Å^2]	1.5(2)	2.0(2)	1.6(2)	1.5(2)
O3 4e(x y z)				
x	0.1988(18)	0.1979(14)	0.2058(13)	0.2065(3)
y	0.1941(13)	0.1940(12)	0.1981(1)	0.2027(2)
z	0.9607(12)	0.9631(9)	0.9687(7)	0.9593(1)
B [Å^2]	0.09(14)	0.23(13)	0.03(13)	1.4(2)
χ^2	8.10	3.65	4.33	2.91
R_p (%)	4.48	3.58	3.58	2.98
R_{wp} (%)	5.77	4.58	4.97	3.83
R_I (%)	5.41	4.39	6.65	4.94
$R_{mag.}$ (%)	4.62	6.18	6.81	9.79

[a] The Fe/W occupancy factors were determined from XRPD data and fixed in the refinement of the NPD data.

Table 3 lists the main interatomic distances and angles in the series. A reduction of the <B–O> and <B′′–O> distances is observed when x increases as this corresponds to the progressive oxidation of Fe^{2+} to Fe^{3+}. For the same reason, the superexchange <B′–O–B′′> angle increases progressively with the tolerance factor of the perovskites upon replacement of Fe^{2+} by Fe^{3+}. Brown's phenomenological Bond-Valence Model (BVS)[19] can also help to give an estimation of the actual valence of Fe cations by means of an empirical relationship between the observed bond lengths (Table 3) and the valence of a bond. This calculation can only be applied to the 2d sites for x = 0.2 and 0.23 that do not contain a mixed Fe/W occupancy. The valence

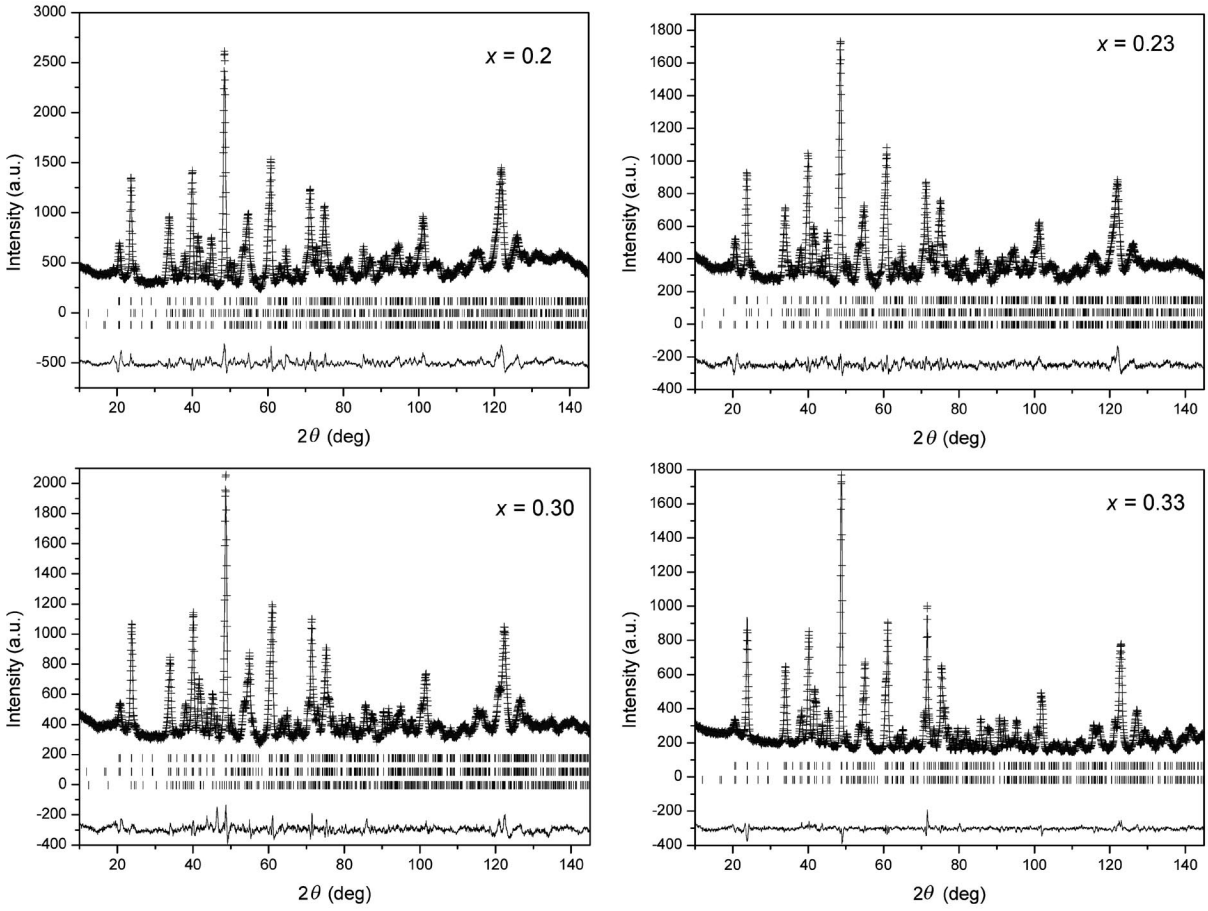

Figure 4. Observed (crosses), calculated (full line) and difference (bottom) NPD Rietveld profiles at 295 K for the $Ca_2Fe_{1+x}W_{1-x}O_6$ samples (x = 0.2, 0.23, 0.3 and 0.33). The three sets of reflection markers correspond to the main phase, the minor impurity $Ca_2Fe_2O_5$ (x = 0.2, 0.23 and 0.3) or $CaWO_4$ (x = 0.33) and the magnetic structure.

is the sum of the individual bond valences (s_i), which are calculated as $s_i = \exp[(r_0 - r_i)/0.37]$, where r_0 for the Fe^{2+}–O^{2-} pair is 1.734. The bond valences of Fe at 2d sites are +2.62(3) and +2.72(3) for x = 0.20 and x = 0.23, respectively, in good agreement with the nominal oxidation states, of +2.67 and +2.75, respectively (Table 1).

Table 3. Main interatomic distances [Å] and angles [°] for $Ca_2Fe_{1+x}W_{1-x}O_6$ (x = 0.2, 0.23, 0.3 and 0.33) at room temp. for the cations in the B′ (2*d*) and B′′ (2*b*) positions.

	x = 0.2	x = 0.23	x = 0.3	x = 0.33
B′O_6 octahedra				
B′–O1 (×2)	2.048(13)	2.015(12)	1.9973(10)	1.9895(15)
B′–O2 (×2)	2.041(10)	2.034(9)	2.0299(9)	1.9800(15)
B′–O3 (×2)	2.035(8)	2.029(7)	2.0236(7)	2.0078(13)
<B′–O>	2.041	2.026	2.017	1.995
B′′O_6 octahedra				
B′′–O1 (×2)	1.946(13)	1.977(12)	1.9789(10)	1.9640(15)
B′′–O2 (×2)	1.974(10)	1.988(9)	1.9945(9)	1.9940(13)
B′′–O3 (×2)	1.985(9)	1.985(7)	1.9524(7)	1.9679(15)
<B′′–O>	2.013	2.011	1.975	1.973
Angles around O				
B′–O1–B′′	151.1(5)	151.2(5)	152.10(5)	153.73(6)
B′–O2–B′′	151.0(4)	149.9(4)	147.73(4)	152.84(6)
B′–O3–B′′	150.3(3)	150.7(3)	154.18(3)	152.64(6)
<B′–O–B′′>	150.8	150.6	151.3	153.0

Magnetic Measurements

The *dc* susceptibility vs. temperature data of $Ca_2Fe_{1+x}W_{1-x}O_6$ samples for two extreme x values (x = 0.2 and 0.33) are displayed in Figure 5. The susceptibility increases progressively below 330 K for x = 0.33 ($Ca_3Fe_2WO_9$), displaying the spontaneous evolution characteristic of a ferro- or ferrimagnet. The T_C of 330 K is obtained from the derivative of the susceptibility. In contrast, the sample with the higher quantity of Fe^{2+} (x = 0.2) seems to show a T_C above 400 K, although the present data are limited to 400 K. This large T_C can be considered to be a direct consequence of the higher degree of order existing between the cations in B′ and B′′ sites as the amount of Fe^{2+} increases. It is evident that the long-range order of Fe cations in the B sub-lattice favors the magnetic interactions, thus increasing the magnetic ordering temperature. Although the reciprocal susceptibility for x = 0.33 does not show a perfectly linear plot in the highest temperature

range ($360 < T < 400$ K, see inset of Figure 5), a trial fit to a Curie–Weiss law gives a characteristic paramagnetic temperature, Θ_{Weiss}, of 300(1) K, thereby suggesting the presence of strong ferromagnetic interactions, and a value for the effective paramagnetic moment, μ_{eff}, of 4.86(1) μ_B/f.u. Assuming the electronic configuration $Fe^{3+}(3d^5)$–$W^{6+}(5d^0)$, this magnetism only arises from trivalent Fe ($S = 5/2$). An expected paramagnetic moment of 6.83 μ_B/f.u. should be obtained for the formula $Ca_2Fe_{1.33}W_{0.66}O_6$ in the absence of short-range magnetic interactions. These conditions are certainly not accomplished immediately above T_C.

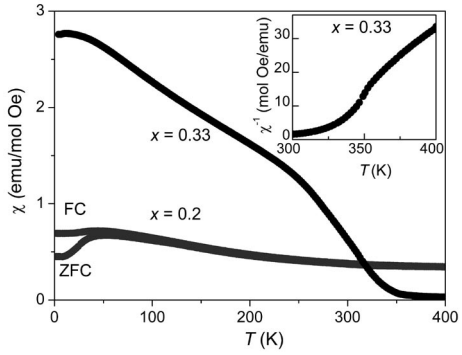

Figure 5. Plot of magnetization vs. temperature ($H = 1000$ Oe) for $Ca_2Fe_{1+x}W_{1-x}O_6$ ($x = 0.2$ and 0.33). The inset shows the reciprocal susceptibility for $x = 0.33$ above room temperature.

The isothermal magnetization curves for $x = 0.2$ and 0.33 are displayed in Figure 6. A saturation magnetization of 0.36 μ_B/f.u. is reached for the sample with $x = 0.2$ at the maximum applied field of 50 kOe. A saturation magnetization (extrapolating to H = 0) of 1.12 μ_B/f.u., with a maximum magnetization of 1.85 μ_B/f.u., is reached for $x = 0.33$. As shown in the inset of Figure 6, the hysteresis cycle for $x = 0.33$ is very narrow, with a coercive field of 470 Oe, characteristic of a soft ferrimagnetic system.

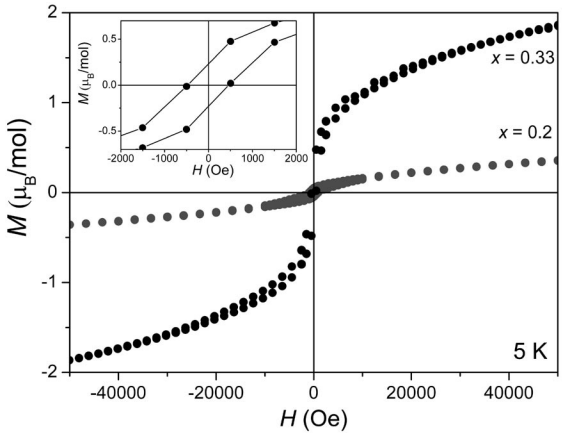

Figure 6. Plot of magnetization vs. magnetic field ($T = 5$ K) for $Ca_2Fe_{1+x}W_{1-x}O_6$ ($x = 0.2$ and 0.33). The inset shows the coercive field for the $x = 0.33$ sample.

Magnetic Structure

All the compounds studied by neutron diffraction are magnetically ordered at room temperature and show a magnetic contribution to the scattering at allowed Bragg positions ($k = 0$), mainly on the (011) reflection, as this corresponds to a ferro- or ferrimagnetic long-range ordering. We modeled the magnetic structure for all these compounds as a ferrimagnetic arrangement of Fe spins with alternating directions at 2d and 2*b* sites, with the moments lying along the *c* direction. We also constrained the scale factors of both structural and magnetic models and refined the magnitude of the ordered Fe magnetic moments at both crystallographic positions. The Rietveld fits at 295 K, as shown in Figure 4, include the magnetic contributions to the scattering as a second phase. Table 2 shows the value of the Fe magnetic moments at room temperature. The value of the Fe magnetic moment for the $x = 0.2$, 0.23 and 0.3 samples is higher than the Fe magnetic moment for $x = 0.33$. This is because the samples with smaller x are still strong ferromagnets at room temperature whereas the observed T_C (330 K) for $x = 0.33$ occurs at only slightly above room temp.

An NPD study at 4 K was also carried out for the end of the series $Ca_2Fe_{1+x}W_{1-x}O_6$ with $x = 0.33$ in order to investigate its magnetic structure at low temperature. The inset of Figure 7 shows the magnitude of the main magnetic reflection at 4 K compared with the NPD diagram at 295 K. The magnetic structure was refined with the same model described previously for the patterns at room temperature. The values of the Fe magnetic moments obtained at 4 K are 2.5(1) μ_B at the 2d position and –1.3(1) μ_B at the 2*b* site. Both values are significantly higher than those obtained at room temperature (Table 2) since the magnetic structure is fully established at 4 K. The goodness of fit is illustrated in Figure 7, where the second row of allowed Bragg reflections corresponds to the $CaWO_4$ impurity and the third row to the magnetic structure. The agreement factors were: $R_p = 4.05\%$, $R_{wp} = 5.10\%$, $R_{exp} = 2.11\%$, $\chi^2 =$

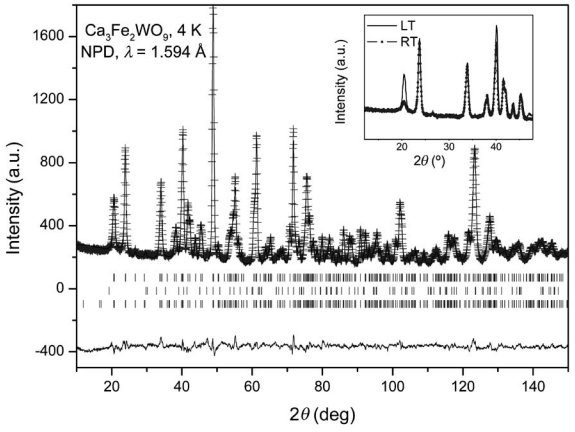

Figure 7. Observed (crosses), calculated (full line) and difference (bottom) NPD Rietveld profiles at 4 K for $Ca_2Fe_{1.33}W_{0.67}O_6$ (or $Ca_3Fe_2WO_9$). The inset shows the low angle region of the NPD patterns at 4 K (full line) and room temperature (dotted line).

5.83, R_{Bragg} = 6.43%, R_{mag} = 5.64%. A view of the magnetic structure, which can be described as a stacking of ferromagnetic layers of antiferromagnetically coupled Fe spins along the [101] direction, is shown in Figure 8. The magnetic structure described here is simpler than that described previously for $Ca_3Fe_2WO_9$,[16] which required a propagation vector (1/2,0,1/2), and thus a doubled magnetic unit cell, along the *a* and *c* directions, although they both describe the same magnetic arrangement.

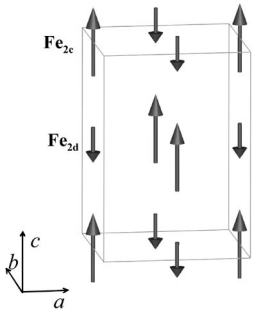

Figure 8. Schematic view of the magnetic structure of $Ca_2Fe_{1.33}W_{0.67}O_6$ ($Ca_3Fe_2WO_9$), where the crystallographic and the magnetic cell coincide (k = 0). Only the magnetic atoms are represented.

Discussion

We have obtained eight oxides of the new series $Ca_2Fe_{1+x}W_{1-x}O_6$, where the average oxidation state of Fe progressively increases from +2.46 for x = 0.13 to +3 for x = 0.33. All of these compounds crystallize in a monoclinically distorted perovskite lattice containing three nonequivalent oxygen atoms, the positions of which were accurately determined by NPD despite the strong pseudo-symmetry present in the structure. In fact, the monoclinic beta angle is very close to 90° in all cases (see Table 2), thereby indicating a strong pseudo-orthorhombic character of the unit cell. Several examples of monoclinically distorted 1:1 ordered perovskites, for example Nd_2MgTiO_6,[20] Ca_2CaUO_6,[21] Sr_2MnWO_6, Ca_2MnWO_6 and Sr_2MnMoO_6,[22] have been described in the past. All these compounds crystallize in the space group $P2_1/n$, with $\mathbf{a} \approx \mathbf{b} \approx \sqrt{2}\mathbf{a_0}$ and $\mathbf{c} \approx 2\mathbf{a_0}$, and show long-range ordering of the two different cations placed at the B positions of the $A_2B'B''O_6$ perovskite structure. The driving force for this B′, B″ ordering is the charge difference between both kinds of cations, for instance Mg^{2+} and Ti^{4+} in Nd_2MgTiO_6, or Mn^{2+} and W^{6+} in Ca_2MnWO_6. In the present case, the charge difference varies smoothly from the first members of the series, which have values slightly smaller than four valence units and are fully ordered, to three valence units for the x = 0.33 compound, which presents a rather disordered distribution of Fe^{3+} and W^{6+} over the two octahedral sub-lattices. The evolution of the antisite disordering has a dramatic influence on the magnetic properties across the series.

In contrast with other ferrimagnetic double perovskites where the B″ cation has itinerant electrons that participate in the magnetic coupling, the only possible magnetic superexchange mechanism for the present $Ca_2Fe_{1+x}W_{1-x}O_6$ system, which nominally contains only Fe^{2+}–Fe^{3+} and W^{6+}, occurs via Fe_{2d}–O–Fe_{2b} paths in Fe-rich areas of the crystal containing neighboring Fe spins. Figure 9 shows a simplified image of the magnetic ordering in two selected extreme compositions (x = 0.2 and x = 0.33); only one layer of B cations is shown for the sake of simplicity. For x = 0.2 (Figure 9, a), the 2*d* sites contain 100% Fe whereas the 2*b* positions contain 20% Fe; for x = 0.33 (Figure 9, b), the 2*d* sites contain 78% Fe whereas the 2*b* positions show a 55%/45% random distribution of Fe and W.

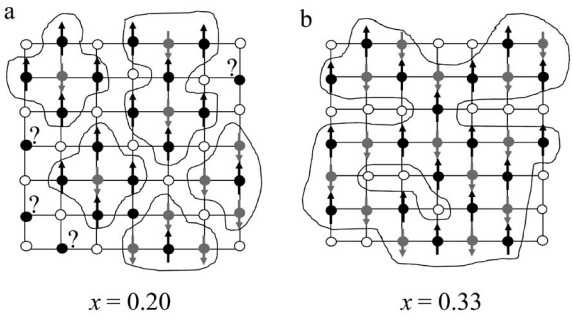

Figure 9. Ideal schematic view of the magnetic coupling in $Ca_2Fe_{1+x}W_{1-x}O_6$ (x = 0.20 and 0.33). The x = 0.2 compound contains Fe atoms at 2*d* positions (black atoms and spins) and randomly distributed Fe (grey atoms and spins) and W (white atoms) at the 2*b* positions. AFM magnetic coupling is via Fe–O–Fe pathways (along the lines). Naturally occurring Fe-rich patches are antiferromagnetically coupled, and there is some magnetic coherence between adjacent patches. For x = 0.33 there are randomly distributed Fe (black atoms and spins at 2*d* and grey atoms and spins at 2*b* sites) and W atoms (white) at both octahedral positions; there is an almost full magnetic coherence across the crystal.

For x = 0.2, which only contains 20% of Fe at the 2*b* positions, it is clear that full magnetic coherence is not reached across the crystal, which contains isolated islands of several antiferromagnetically coupled Fe atoms below the ordering temperatures. As illustrated in Figure 9, the coupling between near-neighbour Fe_{2d}–O–Fe_{2b} cations is always AFM. The strength of these Fe_{2d}–O–Fe_{2b} superexchange AFM interactions is comparable to those existing in $RFeO_3$ ferrites (R = rare earths), which account for the high T_C (>400 K) observed for this compound. However, the lack of coherence between isolated AFM patches explains the weak saturation magnetization observed for the x = 0.2 perovskite. This lack of coherence recalls the features of a spin-glass-like state, as also suggested by the divergence of the ZFC and FC susceptibility curves at low temperatures (Figure 5). It can be helpful to remember that the double perovskite Sr_2FeWO_6, where every $Fe^{2+}O_6$ octahedron is surrounded by six $W^{6+}O_6$ octahedra, is an antiferromagnet only below 37 K[7] due to a weak super-super-exchange mechanism across Fe–O–W–O–Fe paths. In the present case, the presence of 0.2 Fe atoms at the 2*b* positions accounts for an extraordinary enhancement of the magnetic coupling strength involving first-neighbor interactions, although this effect does not concern all the Fe atoms in the crystal.

For $x = 0.33$, a perfect ferrimagnetic coupling between up Fe^{3+} spins at 2*d* sites (black in Figure 9, b) and down Fe^{3+} spins at 2*b* positions (grey in Figure 9, b) would ideally give a net magnetization of $5 \times (0.78–0.55) = 1.15\ \mu_B$/f.u., which is very close to the observed saturation magnetization (Figure 6). This magnetization is also compatible with the ordered magnetic moments of 2.5 μ_B for 2*d* and –1.3 μ_B for 2*b* sites, which yields a difference of 1.2 μ_B, observed at 4 K by neutron diffraction. This situation would require a perfect coherence between Fe-rich patches, and an almost full coherence is indeed reached for the degree of disordering existing in both sub-lattices (see Figure 9, b). For a cubic lattice, where the 2*d* positions are 78% occupied by Fe ions and the 2*b* sites are statistically 55% occupied by Fe cations, the long-range magnetic connections through Fe_{2d}–O–Fe_{2b}–O–Fe_{2d} largely exceed the 31% percolation limit of a simple cubic lattice. The monoclinic distortion observed here does not change these considerations.

It is worth comparing the low-temperature magnetic structure of $Ca_3Fe_2WO_9$ with that reported for the related $Sr_3Fe_2WO_9$ oxide,[23] which shows a tetragonal *I*4/*m* symmetry. The Ca compound shows an antiferromagnetic arrangement of Fe^{3+} spins at the 2*d* and 2*b* positions, with a moderately ordered moment at 2*d* sites (2.5 μ_B) with respect to 2*b* positions (–1.3 μ_B), whereas the Sr perovskite shows ordered magnetic moments of 4.16 μ_B and –3.49 μ_B at 2*a* and 2*b* sites at 10 K, according to neutron diffraction data. In both cases, however, there is a considerable disordering between Fe and W over both crystallographic positions. As observed in $Ca_3Fe_2WO_9$, the high structural disordering observed leads to an enhancement of the magnetic interactions between B′ and B′′ sites, as evidenced by the high Curie temperatures (T_C = 330 and 373 K for Ca and Sr, respectively). The fact that the value of the ordered magnetic moments is much higher in the Sr compound is certainly related to the more open superexchange angles observed in the tetragonal $Sr_3Fe_2WO_9$ structure (Fe–O–Fe angles of 180° along the *c*-direction and 174° in the *ab* plane), with respect to the average <Fe–O–Fe> angle of 153° (at room temp.) determined for $Ca_3Fe_2WO_9$, which also accounts for the weaker magnetic interactions.

Conclusions

The study of the crystal structures of the double perovskites $Ca_2Fe_{1+x}W_{1-x}O_6$ (x = 0.2, 0.23, 0.30, 0.33) from neutron powder diffraction data shows a room temperature monoclinic structure, space group $P2_1/n$, for all of them, with increasing degrees of antisite disorder as the average oxidation state of Fe increases along the series. All these compounds are magnetically ordered at room temperature, with the magnetic structure being defined by the propagation vector $k = 0$ and described as a stacking of ferromagnetic layers of antiferromagnetically coupled Fe spins along the [101] direction. The $x = 0.33$ perovskite shows the same magnetic structure at 4 K. The increasing Fe content across the series implies an evolution from a scenario where the antiferromagnetic patches are isolated, which leads to a low macroscopic saturation magnetization, to a model where the Fe-rich patches, which are strongly coupled via Fe–O–Fe superexchange interactions, present an excellent coherence across the crystal, thus yielding the expected saturation magnetizations according to the observed antisite disorder and a strong magnetic scattering on the low-angle Bragg positions.

Experimental Section

Eight oxides belonging to the series $Ca_2Fe_{1+x}W_{1-x}O_6$ were prepared as black polycrystalline powders from stoichiometric amounts of analytical grade $CaCO_3$, $FeC_2O_4{\cdot}2H_2O$ and $H_{24}N_6O_{39}W_{12}{\cdot}18H_2O$, which were dissolved in citric acid by adding several drops of concentrated HNO_3. The obtained resins were dried at 120 °C and further decomposed at 600 °C, then ground and fired at 800 °C to eliminate organic materials and nitrates. The precursors were then treated under different conditions to obtain the different members of the $Ca_2Fe_{1+x}W_{1-x}O_6$ series. The material $Ca_2Fe_{1.33}W_{0.66}O_6$ (also rewritten as $Ca_3Fe_2WO_9$) was stabilized by heating the precursors in air at 1000 °C for 12 h, whereas different reducing flows were used to obtain the remaining members of the series, in this case H_2(5%)/N_2(95%) at different synthesis temperatures of between 700 and 950 °C.

The products were initially characterized by XRPD (Cu-K_α, λ = 1.5406 Å) for phase identification and to evaluate phase purity. For the structural refinements, NPD patterns of selected samples were collected at room temperature at the high-resolution D2B neutron diffractometer at ILL-Grenoble in high-flux mode. About 4 g of sample were placed in a vanadium can, and a collecting time of 3 h was required for each pattern. A wavelength of 1.594 Å was selected from a Ge monochromator. The patterns were refined by the Rietveld method, using the FULLPROF refinement program.[24] A pseudo-Voigt function was chosen to generate the line shape of the diffraction peaks. No regions were excluded in the refinement. The following parameters were refined from the D2B data in the final run: scale factor, background coefficients, zero-point error, unit-cell parameters, pseudo-Voigt corrected for asymmetry parameters, positional coordinates, isotropic atomic displacement parameters, and magnitudes of the Fe magnetic moments.

The *dc* magnetic susceptibilities were measured with a commercial SQUID magnetometer for powdered samples in the temperature range 1.5–700 K and fields of up to 6 T.

Acknowledgments

We are grateful for financial support from the Spanish Ministerio de Ciencia y Tecnología (MCYT) (grants no. MAT2007-60536 and MAT2008-06517-C02-01) and the Argentinean Agencia Nacional de Promoción Científica y Tecnológica (ANPCYT) (grant no. PICT 25459), the Secretaría de Ciencia y Técnica de la Universidad Nacional de San Luis (SECYT-UNSL) (grant no. 7707), and the Consejo Nacional de Investigaciones Científicas y Técnicas (CONICET) (PIP no. 6246). We are also grateful to the Institut Laue Langevin for allowing us to use their facilities. C. A. L. is grateful for a CONICET fellowships and J. C. P. is a member of CONICET.

[1] K. I. Kobayashi, T. Kimura, H. Sawada, K. Terakura, Y. Tokura, *Nature* **1998**, *395*, 677.

[2] M. Anderson, K. B. Greenwood, G. A. Taylor, K. R. Poeppelmeier, *Prog. Solid State Chem.* **1993**, *22*, 197.
[3] P. Woodward, R. D. Hoffman, A. W. Sleight, *J. Mater. Res.* **1994**, *9*, 2118.
[4] C. Ritter, M. R. Ibarra, L. Morellón, J. Blasco, J. García, J. M. de Teresa, *J. Phys.: Condens. Matter* **2000**, *12*, 8295.
[5] T. H. Kim, M. Uehara, S.-W. Cheong, Y. S. Lee, *Appl. Phys. Lett.* **1999**, *74*, 1737.
[6] K. I. Kobayashi, T. Kimura, Y. Tomioka, H. Sawada, K. Terakura, *Phys. Rev. B* **1999**, *59*, 11159.
[7] D. Sanchez, J. A. Alonso, M. G. Hernandez, M. J. Martinez-Lope, J. L. Martinez, A. Mellergard, *Phys. Rev. B* **2002**, *65*, 104426.
[8] R. I. Dass, J. B. Goodenough, *Phys. Rev. B* **2001**, *63*, 064417.
[9] S. Ray, A. Kumar, S. Majumdar, E. V. Sampathkumaran, D. D. Sarma, *J. Phys.: Condens. Matter* **2001**, *13*, 607.
[10] Z. M. Fu, W. X. Li, *Sci. China, Ser. A* **1995**, *38*, 974.
[11] J. A. Alonso, M. T. Casais, M. J. Martinez-Lope, J. L. Martinez, P. Velasco, A. Muñoz, M. T. Fernández-Díaz, *Chem. Mater.* **2000**, *12*, 161.
[12] W. Prellier, V. Smolyaninova, A. Biswas, C. Galley, R. L. Greene, K. Ramesha, J. Gopalakrishanan, *J. Phys.: Condens. Matter* **2000**, *12*, 965.
[13] R. M. Pinacca, M. C. Viola, J. A. Alonso, J. C. Pedregosa, R. E. Carbonio, *J. Mater. Chem.* **2005**, *15*, 4648.
[14] M. C. Viola, J. A. Alonso, J. C. Pedregosa, R. E. Carbonio, *Eur. J. Inorg. Chem.* **2005**, 1559.
[15] M. S. Ausburger, M. C. Viola, J. C. Pedregosa, R. E. Carbonio, *J. Mater. Chem.* **2006**, *16*, 4235.
[16] S. A. Ivanov, S. G. Eriksson, R. Tellgren, H. J. Rundlof, *J. Solid State Chem.* **2005**, *178*, 3605.
[17] R. D. Shannon, *Acta Crystallogr., Sect. A* **1976**, *32*, 751.
[18] C. J. Howard, B. J. Kennedy, P. M. Woodward, *Acta Crystallogr., Sect. B* **2003**, *59*, 463.
[19] N. E. Brese, M. O'Keefe, *Acta Crystallogr., Sect. B* **1991**, *47*, 192.
[20] W. A. Groen, F. P. F. Van Berkel, D. J. W. Ijdo, *Acta Crystallogr., Sect. C* **1986**, *42*, 1472.
[21] H. C. Van Duivenboden, D. J. W. Ijdo, *Acta Crystallogr., Sect. C* **1986**, *42*, 523.
[22] A. Muñoz, J. A. Alonso, M. T. Casais, M. J. Martínez-Lope, M. T. Fernández-Díaz, *J. Phys.: Condens. Matter* **2002**, *14*, 8817.
[23] S. A. Ivanov, S. G. Eriksson, R. Tellgren, H. Rundlof, *Mater. Res. Bull.* **2001**, *36*, 2585.
[24] J. Rodríguez-Carvajal, *Phys. B* **1993**, *192*, 55.

Received: March 18, 2009
Published Online: July 22, 2009

